A RELATIONSHIP BETWEEN AGN JET POWER AND RADIO POWER

K. CAVAGNOLO[1,6], B. MCNAMARA[1,2,3], P. NULSEN[3],
C. CARILLI[4], C. JONES[3], & L. BÎRZAN[5],

For submission to ApJ

ABSTRACT

Using X-ray data collected with the *Chandra* X-ray Observatory and multi-frequency VLA radio data, we investigate the scaling relationship between active galactic nucleus jet power, $P_{\rm jet}$, and observed radio power, $P_{\rm radio}$. We seek to determine if the $P_{\rm jet}$-$P_{\rm radio}$ scaling relations presented in Bîrzan et al. (2008) for, primarily, brightest cluster galaxies (BCGs) are continuous in form and scatter from giant elliptical galaxies (gEs) up to BCGs. We expand the sample used in Bîrzan et al. (2008) to lower radio power by incorporating measurements for 21 gEs. Combining our results with those presented in Bîrzan et al. (2008), we find a mean scaling relation of $P_{\rm jet} \approx 4 \times 10^{16}\ P_{\rm radio}^{0.68}$ erg s^{-1} with a scatter of ≈ 0.7 dex. We briefly comment on the consistency of our results with theoretical models, specifically those of Blandford & Konigl (1979) and Willott et al. (1999). Our results are consistent with models for confined radio sources that are close to minimum energy density, with the ratio of lobe energy in neutralizing species to that in relativistic electrons of $\gtrsim 100$. We also discuss the importance of environment when measuring a $P_{\rm jet}$-$P_{\rm radio}$ relation, and a possible connection to the process of entrainment. A brief discussion of the implications and utility of our results for large-scale structure formation models is also included.

Subject headings: galaxies: active – galaxies: clusters: general – X-rays: galaxies – radio continuum: galaxies

1. INTRODUCTION

Observational evidence accumulated over the last decade indicates that most galaxy bulges harbor a central supermassive black hole (SMBH). It has been suggested that SMBHs co-evolved with the host galaxy, giving rise to the well-known correlations between bulge luminosity, stellar velocity dispersion, and central black hole mass (Kormendy & Richstone 1995; Magorrian et al. 1998; Ferrarese & Merritt 2000; Gebhardt et al. 2000; Marconi & Hunt 2003; Best et al. 2005). Models also suggest that these correlations were imprinted by co-evolution through galaxy mergers and by the influence of feedback from active galactic nuclei (AGN) (*e.g.* Silk & Rees 1998; Kauffmann & Haehnelt 2000). Around the same time, the *Chandra* X-ray Observatory (Weisskopf et al. 2000) found direct evidence for AGN feedback when observations unambiguously revealed AGN induced cavities and shock fronts in the X-ray emitting gas surrounding many massive galaxies (*e.g.* McNamara et al. 2000; Fabian et al. 2000; Schindler et al. 2001).

It was recognized that X-ray cavities provide an unambiguous gauge of the total mechanical energy and mean jet power produced by SMBHs (McNamara et al. 2000). Jet powers, $P_{\rm jet}$, are approximated using estimates of cavity age and measurement of the pV work done by an AGN in excavating a cavity (see Peterson & Fabian 2006; McNamara & Nulsen 2007, for a reviews). It is important to note that cavity power, $P_{\rm cav}$, is the measured quantity and it is assumed to be a good estimate of the physical quantity $P_{\rm jet}$. Several detailed studies of cavities have shown that AGN feedback supplies enough energy to regulate star formation and suppress cooling of the hot halos of galaxies and clusters (Bîrzan et al. 2004; Dunn et al. 2005; Rafferty et al. 2006; Dunn & Fabian 2008; Bîrzan et al. 2008; Diehl & Statler 2008). Likewise, the existence of correlations between low core entropy, short central cooling time, cooling luminosity, and $P_{\rm jet}$ indicate the presence of a finely-tuned environmental feedback loop (*i.e.* Cavagnolo et al. 2008; Rafferty et al. 2008; Cavagnolo et al. 2009; Mittal et al. 2009; Sanderson et al. 2009)

The mounting observational evidence has changed our view of galaxy formation. A consensus has emerged that AGN feedback plays an important role in suppressing star formation in bulges at late times. Including energetic feedback from AGN in numerical simulations has been shown to bring the shape and normalization of the galaxy luminosity function into better agreement with observations (Croton et al. 2006; Bower et al. 2006; Saro et al. 2006; Sijacki et al. 2007). However, the details of how AGN couple to their ambient environments remain poorly understood (De Young et al. 2008; Mathur et al. 2009). A long-standing problem with extragalactic radio sources has been finding a method to reliably measure their total mechanical output, which is central to understanding AGN feedback (*e.g.* Rawlings & Saunders 1991; Ledlow & Owen 1996).

Individual studies of X-ray cavities have yielded reliable constraints on AGN energetics, ages, and radio lobe composition. But, the systematic study of large samples of cavities has been restricted by observational limitations such as the need for long exposure times and high spatial resolution (Bîrzan et al. 2009). Therefore, measuring and calibrating correlations between simple observables, like AGN radio power ($P_{\rm radio}$), and jet power (*e.g.* $P_{\rm jet}$) in bright, relatively nearby objects will enable more statistical studies of feedback in galaxies, groups, and clusters that are beyond the grasp of current X-ray instrumentation. A robust $P_{\rm jet}$-$P_{\rm radio}$ scaling relation could then be applied to measurements from current and future all-sky radio surveys (*e.g.* NVSS, SUMSS, LOFAR, SKA) to study SMBH formation history and subsequent AGN mechanical heating of the Universe (Croton et al. 2006;

[1] Department of Physics and Astronomy, University of Waterloo, Waterloo, ON N2L 3G1, Canada.
[2] Perimeter Institute for Theoretical Physics, 31 Caroline Street N, Waterloo, ON N2L 2Y5, Canada.
[3] Harvard-Smithsonian Center for Astrophysics, 60 Garden Street, Cambridge, MA 01238, USA.
[4] National Radio Astronomy Observatory, P.O. Box 0, Socorro, NM 87801-0387, USA.
[5] Leiden Observatory, University of Leiden, P.O. 9513, 2300 RA Leiden, The Netherlands
[6] kcavagno@uwaterloo.ca

Sijacki & Springel 2006).

Observational relationships between $P_{\rm jet}$ and $P_{\rm radio}$ for samples of, primarily, BCGs were presented in Bîrzan et al. (2004, hereafter B04) and Bîrzan et al. (2008, hereafter B08). In B08, scaling relations between $P_{\rm jet}$ and 327 MHz, 1.4 GHz, and bolometric radio luminosities were presented. B08 showed that $P_{\rm jet} \propto P_{\rm radio}^{0.5-0.7}$ depending on the choice of frequency. However, there are few objects in the B08 study with $P_{\rm radio} \lesssim 10^{38}$ erg s^{-1} and $P_{\rm jet} \lesssim 10^{43}$ erg s^{-1}, *i.e.* the region generally populated by low-power radio galaxies.

In this paper we extend the study of B08 with the inclusion of 21 gEs from systems with lower X-ray luminosities than rich clusters. Combining the B08 results and the results in this paper, we find a relationship between jet power and radio power which is similar at high and low radio frequencies. The relationships span 6-8 orders of magnitude in $P_{\rm jet}$ and $P_{\rm radio}$, and have the general form $P_{\rm jet} \sim 10^{43}(P_{\rm radio}/10^{40})^{0.7}$ erg s^{-1} with dominantly intrinsic scatter of ~ 0.7 dex. We also find encouraging similarity between our best-fit relations, previous studies, and theoretical AGN models.

This paper is structured as follows: §2 outlines the sample of selected gEs. X-ray and radio data reduction is discussed in §3. Results and discussion are presented in §4. The summary and concluding remarks are given in §5. A ΛCDM cosmology with $H_0 = 70\ h_{70}$ km s^{-1} Mpc^{-1}, $\Omega_{\rm M} = 0.27$, and $\Omega_\Lambda = 0.73$ is adopted throughout. All quoted uncertainties are 68% confidence.

2. SAMPLE

Our sample of 21 gEs is taken from the sample of 160 gEs compiled by Jones et al. (in preparation). The B08 sample is taken from Rafferty et al. (2006, hereafter R06). Information regarding our gE sample is listed in Table 1. The Jones et al. compilation is drawn from the samples of Beuing et al. (1999) and O'Sullivan et al. (2003) using the criteria that the K-band luminosity is $> 10^{10}\ L_\odot$ and the object has been observed with *Chandra*. Of the 160 gEs, extended X-ray emission was detected in 109 objects. AGN activity was suspected in 27 objects based solely on the presence of surface brightness depressions in the X-ray emitting gas. We have further excluded dwarf galaxies ($M_V < -19.5$) from the sample since it is not clear that the substructure in the X-ray gas is associated with an AGN, leaving 21 objects. The 21 gEs in our sample are in relatively low density environments, *i.e.* these are not the central dominant or brightest galaxies in clusters or groups. The gEs studied here have X-ray halos and radio sources with luminosities lower than are typically found for cDs and BCGs.

3. OBSERVATIONS AND DATA ANALYSIS

3.1. *X-ray*

Outburst powers are determined in the usual manner from the X-ray data (see B04 and R06). Gas properties used here are taken from the analysis by Jones et al. (in preparation). Cavity locations and sizes are from Nulsen et al. (in preparation), with cavity volumes and their errors calculated by the method of B04. The enthalpy of each cavity is determined as $H_{\rm cav} = [\gamma/(\gamma-1)]pV$, where p is the gas pressure at the radius of the projected center of the cavity, V is cavity volume, and $\gamma = 4/3$ is assumed for the ratio of specific heat capacities within the cavities. To estimate the average power of an outburst, the enthalpy of each cavity is divided by an estimate of its age. These power estimates are summed for all the cavities in each system to obtain an estimate of the average outburst power of its AGN. For compatibility with B08, here we give results only for the buoyancy age estimates, $t_{\rm buoy}$. Because the uncertainties are large (chiefly due to the uncertain volume estimates), errors are propagated in log space assuming that the errors in the observable inputs p, V, and age are independent of one another.

3.2. *Radio*

Radio powers were estimated using the relation $\nu_0 L_{\nu_0} = 4\pi D_L^2 (1+z)^{\alpha-1} S_{\nu_0} \nu_0$, where S_{ν_0} is the flux density at the observed frequency, ν_0, over the integrated area of the source, z is redshift, D_L is luminosity distance, and α is radio spectral index. The radio powers estimated using 200-400 MHz and 1.4 GHz fluxes are denoted as $P_{200-400}$ and $P_{1.4}$, respectively. The redshift dependent α correction in $\nu_0 L_{\nu_0}$ is small for our sample since the objects are nearby. We have assumed the radio spectra behave as $S_\nu \propto \nu^{-\alpha}$ with a spectral index of $\alpha = 0.8$, typical for extragalactic radio galaxies (Condon 1992).

The 1.4 GHz continuum radio flux for each source was taken from the flux-limited NRAO VLA Sky Survey (NVSS, Condon et al. 1998). For NGC 1553, which lies outside the NVSS survey area, the 843 MHz continuum radio flux was taken from the Sydney University Molonglo Sky Survey (SUMSS, Bock et al. 1999; Mauch et al. 2003). The 1.4 GHz flux for N1553 was estimated using $\alpha = 0.89$, which was calculated from the 843 MHz SUMSS flux and 5 GHz Parkes flux (Whiteoak 1970).

The radio morphologies for our sample are heterogeneous: some sources are large and extended, while others are compact. To ensure the entire radio source was measured, a fixed physical aperture of 1 Mpc was searched around the X-ray centroid of each target. For each target field, all detected radio sources were overlaid on a composite image of X-ray, optical (DSS I/II[7]), and infrared emission (2MASS[8]). When available, the deeper and higher resolution radio data from VLA FIRST[9] was included. A visual inspection was then performed to establish which radio sources were associated with the target gE. After confirming which radio sources within the search region were associated with the target gE, the fluxes of the individual sources were added and the associated uncertainties summed in quadrature.

Archival VLA data for each source in the sample was also reduced and analyzed. The continuum VLA data was reduced using a customized version of the NRAO VLA Archive Survey[10] reduction pipeline. In the cases where high-resolution VLA archival data is available, multifrequency images were used to confirm the connection between NVSS detected radio sources and the host gE. Images at 1.4 GHz were further used to check NVSS fluxes. We found flux agreement for most sources, the exceptions being IC 4296 and NGC 4782, where the NVSS flux is approximately a factor of 2 lower. These sources are unique because the radio lobes contain significant power in diffuse, extended emission which is not detected in NVSS. For these sources, the fluxes measured from the archival VLA data are used in our analysis. The additional data analysis step was also used to investigate the poorly confined sources discussed in Section §4. For the systems where

[7] http://archive.stsci.edu/dss/
[8] http://www.ipac.caltech.edu/2mass/
[9] http://sundog.stsci.edu
[10] http://www.aoc.nrao.edu/∼vlbacald

nuclear radio emission was resolved, we found, on average $S_{\nu_0,\rm nucleus}/S_{\nu_0,\rm total} \lesssim 0.1$, suggesting the nuclear contribution to the low-resolution NVSS measurements has a negligible impact on our results.

B08 found that using lower frequency radio data, *i.e.* 327 MHz versus 1400 MHz, resulted in a lower scatter $P_{\rm jet}$-$P_{\rm radio}$ relation. For our sample of gEs, the quality and availability of 327 MHz data were not ideal, and thus we gathered low-frequency radio fluxes from the CATS Database[11] (Verkhodanov et al. 1997). The CATS Database is a compilation of more than 350 various radio catalogs (*e.g.* WENSS, WISH, TXS, B3). CATS was queried for low frequency counterparts to the the NVSS and SUMMS sources. Fluxes in the frequency range 200-400 MHz were then retrieved from the returned lists. Of the 21 gEs in our sample, 17 of them were found to have radio sources in the CATS database with measured fluxes in the 200-400 MHz range.

Our approach for searching CATS implies that objects with low-frequency radio emission but without a higher frequency counterpart will not be included in our sample. However, because CATS does not provide images for visual inspection, and is composed of catalogs having a wide variety of spatial resolutions and flux limits, our method of using highly-restricted search areas mitigates the inclusion of spurious sources. Therefore, the 200-400 MHz radio powers shown in Figure 1 might underestimate the 200-400 MHz fluxes for these gEs. However, because of the large range of radio powers, a systematic shift by a factor of a few along the $P_{\rm radio}$ axis for all the gE points would not alter the best-fit slope significantly.

4. RESULTS AND DISCUSSION

4.1. $P_{\rm jet}$-$P_{\rm radio}$ *Scaling Relation*

The results from the X-ray and radio data analysis are shown in the plots of $P_{\rm cav}$-$P_{1.4}$ and $P_{\rm cav}$-$P_{200-400}$ presented in Figure 1. A subjective figure of merit (FM) was assigned to each set of cavities – shown as color coding in Figure 1 and listed in Table 1. We assigned FMs because no automated algorithm exists for detecting cavities and determining their volumes. The FMs represent our qualitative visual assessment. FM-A cavities are associated with AGN radio activity and have well-defined boundaries; FM-B cavities are associated with AGN radio activity, but lack well-defined boundaries; FM-C cavities have poorly-defined boundaries, and their connection to AGN radio activity is unclear. FM-C cavities are excluded from all fitting, as are a subset of objects we have defined as being poorly confined and which are discussed in Section 4.3.

Figure 1 shows a continuous power law relationship between cavity power and radio power over approximately 8 orders of magnitude in radio power and 6 orders of magnitude in cavity power. To determine the form of the power-law relation, we performed linear fits in log-space for each frequency regime using the bivariate correlated error and intrinsic scatter (BCES) algorithm (Akritas & Bershady 1996). The orthogonal BCES algorithm takes in asymmetric uncertainties for both variables, assumes the presence of intrinsic scatter, and performs a linear least-squares regression which minimizes the squared orthogonal distance to the best-fit relation. This differs from the fitting approach in B08 which minimized the distance in the $P_{\rm cav}$ coordinate. The best-fit parameter uncertainties were calculated using 10,000 Monte Carlo bootstrap resampling trials.

The best-fit orthogonal BCES determined linear function in log-space for the $P_{\rm cav}$-$P_{1.4}$ and $P_{\rm cav}$-$P_{200-400}$ relations are:

$$\log P_{\rm cav} = 0.72\ (\pm 0.13)\ \log P_{1.4} + 1.92\ (\pm 0.17) \quad (1)$$

$$\log P_{\rm cav} = 0.64\ (\pm 0.08)\ \log P_{200-400} + 1.55\ (\pm 0.12) \quad (2)$$

where $P_{\rm cav}$ is in units 10^{42} erg s^{-1}, and $P_{1.4}$ and $P_{200-400}$ are in units 10^{40} erg s^{-1}. The scatter for each relation is $\sigma_{1.4} = 0.77$ dex and $\sigma_{200-400} = 0.61$ dex, and the respective correlation coefficients are $r_{1.4} = 0.73$ and $r_{200-400} = 0.81$. We have quantified the total scatter about the best-fit relation using a weighted estimate of the orthogonal distances to the best-fit line (see Pratt et al. 2009). For comparison, the B08 scaling relations are

$$\log P_{\rm cav} = 0.35\ (\pm 0.07)\ \log P_{1.4} + 1.85\ (\pm 0.10) \quad (3)$$

$$\log P_{\rm cav} = 0.51\ (\pm 0.07)\ \log P_{327} + 1.51\ (\pm 0.12) \quad (4)$$

where $P_{\rm cav}$ is in units 10^{42} erg s^{-1}, and $P_{1.4}$ and P_{327} are in units 10^{24} W Hz^{-1} (or $\approx 10^{40}$ erg s^{-1}). The relations have scatters of $\sigma_{1.4} = 0.85$ dex and $\sigma_{327} = 0.81$ dex. An error in Equation 15 of B08 has been corrected in Equation 4 (Birzan et al. 2010).

In contrast to B08, the slopes of the relations in this work now agree to within their uncertainties. Note that we find a steeper relationship at 1.4 GHz than B08. This difference in slope at 1.4 GHz between our work and B08 is due to the additional data points at lower $P_{\rm jet}$ and the different fitting method. The B08 points tend to be clumped in a fairly narrow power range, which gave the few points at the upper and lower power extremes excessive leverage over the slope. The new data extends to lower jet powers, giving a more uniform sampling and a more robust measurement of the slope and zero point.

As a simple check, we point out two systems with accurate estimates of AGN jet power: Cygnus A and Hercules A. For Cygnus A (point with largest $P_{1.4}$ in Figure 1), where our $P_{\rm jet}$-$P_{\rm radio}$ relations appear to overestimate the jet power by a factor of ≈ 40, the total kinetic luminosity of $\sim 2 \times 10^{46}$ erg s^{-1} calculated by Wilson et al. (2006) using the shock is consistent with the $P_{\rm jet}$ value of $\sim 5 \times 10^{46}$ erg s^{-1} predicted by our relations. Hercules A (which is not in the B08 sample) is a similar case to Cygnus A. With $P_{\rm cav} = 310 \times 10^{42}$ erg s^{-1} and $P_{1.4} = 4100 \times 10^{40}$ erg s^{-1}, Hercules A falls in the same region of Figure 1 as Cygnus A. But, the total kinetic luminosity of $\sim 1.6 \times 10^{46}$ erg s^{-1} calculated by Nulsen et al. (2005) using the shock agrees with the prediction from our relations, $\sim 3.2 \times 10^{46}$ erg s^{-1}.

The substantial scatter in the $P_{\rm jet}$-$P_{\rm radio}$ relations highlight that radio power is an inaccurate surrogate for determining AGN power in individual systems. As seen in systems like Hydra A (Wise et al. 2007) or MS 0735.6+7421 (McNamara et al. 2005), the energetics can be dominated by the effects of an AGN outburst which is more powerful than average. This may be particularly true for gEs, which have lower pressure halos and are more susceptible to disruption by AGN outbursts (Weinmann et al. 2006; Puchwein et al. 2008). B08 showed that correcting for the effect of radio aging by including a scaling with break frequency does reduce the scatter within the relations, but by only $\approx 50\%$.

4.2. *Comparison with Models and Observational Studies*

A multitude of jet models can be found in the literature (*i.e.* Longair et al. 1973; Scheuer 1974; Blandford & Rees 1974; Begelman & Cioffi 1989; Carvalho & O'Dea 2002a,b), and it is beyond the scope of this paper to evaluate all of them.

[11] http://www.sao.ru/cats/

Therefore, we restrict our focus to models which explicitly deal with correlations between jet power and radio emission. We also examine earlier observational studies of $P_{\rm jet}$-$P_{\rm radio}$ other than B08. In this section we use the common parameterization for jet power $P_{\rm jet} = \eta P_{\rm radio}^{\Gamma}$, where $P_{\rm jet}$ is total kinetic jet power, η is some normalization, Γ is a scaling index, and $P_{\rm radio}$ is emergent synchrotron power.

For flat-spectrum compact radio cores (*e.g.* small scale jets and not radio lobes), the jet model by Blandford & Konigl (1979) predicts $\Gamma = 12/17$ (≈ 0.71). Starting with the Blandford & Konigl (1979) model, Falcke & Biermann (1995) found a similar slope when assuming emergent jet power scales with accretion power in a jet-disk system. The more general model for scale-invariant jets by Heinz & Sunyaev (2003) also predicts $\Gamma = 12/17$. Heinz & Grimm (2005) undertook an observational study using 5 GHz core powers and an estimate of $P_{\rm jet}$ from the Galactic X-ray binary mass-radio-X-ray fundamental plane relation (Gallo et al. 2003; Merloni et al. 2003). Fixing $\Gamma = 12/17$, Heinz & Grimm (2005) found $\eta \approx 6 \times 10^{44}$ erg s^{-1} with $P_{\rm radio}$ in units of 10^{40} erg s^{-1}. Utilizing a collection of objects from the R06 sample and 5 GHz core powers corrected for relativistic Doppler boosting, Merloni & Heinz (2007) found that $\Gamma = 0.81$ with $\eta \approx 2 \times 10^{44}$ erg s^{-1} with $P_{\rm radio}$ in units of 10^{40} erg s^{-1}.

Willott et al. (1999, hereafter W99) derive Γ and η using the hypersonic jet model of Falle (1991) assuming radio lobes are at minimum energy density (see Miley 1980, for details). W99 derived $\Gamma = 6/7$ with $\eta \approx f^{3/2}\ 4.61 \times 10^{41}$ erg s^{-1} when $P_{\rm radio}$ is in units of 10^{40} erg s^{-1}. We have adjusted the fiducial W99 normalization from 151 MHz to 1.4 GHz assuming $S_\nu \propto \nu^{-0.8}$. The factor f consolidates a variety of unknowns (see W99 for details). The fiducial W99 model ($f = 1$) yields η two orders of magnitude lower than our best-fit normalizations. Because the W99 model has been widely used for estimating jet power, the difference in η's needs to be explored.

The W99 normalization has a weak dependence on ambient gas density. Using observationally consistent shallower and lower density gas profiles than those used to derive the fiducial W99 model results in faster jet outflow velocities, which in turn increases η by factors of $\sim 2-5$. In addition, the W99 model has a critical dependence on the fractional deviation from the minimum-energy condition and k, which is the ratio of energy in neutralizing species to relativistic electrons. We find that for k lying in the range of tens to hundreds, values consistent with observational findings (Dunn et al. 2005, 2006; De Young 2006; Bîrzan et al. 2008), brings the W99 normalization into agreement with our work. Figure 2 shows that the W99 zero-point lies significantly below our best-fit $P_{\rm jet}$-$P_{\rm radio}$ relations, but the slopes formally agree. W99 find that to fit their model to narrow-line region luminosities (assuming $L_{\rm NLR} \propto P_{\rm jet}$) for sources in the 7C and 3CRR surveys, f must equal 20, which is the upper-limit of f in their model and implies $k \approx 20$.

4.3. *Poorly Confined Sources*

It appears the X-ray data are not deep enough to define the extent of the cavities for several objects in our sample: IC 4296 (Killeen & Bicknell 1988; Pellegrini et al. 2003), NGC 315 (Bridle et al. 1979; Willis et al. 1981), NGC 4261 (Jones & Wehrle 1997; Jones et al. 2000), NGC 4782 (Machacek et al. 2007), and NGC 7626 (Birkinshaw & Davies 1985). For these objects, the X-ray surface brightness decrements are reminiscent of tunnels rather than bubbles, and the radio morphologies are distinctly different from the rest of the gE and B08 objects. X-ray cavities typically enclose the jet+lobe radio emission (see Figure 3 for an example in M84). However, for the PC sources, the only indication of gas excavation in the X-ray halo is found near the base of the jets, seemingly at the "edge" of the X-ray halo (see Figure 3 for an example in NGC 4261). The appearance of breaking-out from the X-ray halo is our reason for suggesting these sources are poorly confined. Because we do not have a robust measurement of $P_{\rm cav}$ for the PC systems, they were excluded from the preceding analysis of the $P_{\rm jet}$-$P_{\rm radio}$ relations.

The observed tunnels do not capture the total $p\,dV$ work being done by the jets. There may well be cavities which are not imaged extending to larger radii and enclosing the radio lobes. But, for PC systems the ambient medium at those radii is too faint to yield a cavity detection. To test this, we calculated $P_{\rm cav}$ values for the PC systems assuming radio lobe morphology approximates the volume of cavities potentially at larger radii. Pressure profiles were extrapolated to large radii using the best-fit parameters of a β-model (Cavaliere & Fusco-Femiano 1978) fit to the surface brightness profile, assuming the ambient atmosphere is isothermal, and adding a background gas pressure of 10^{-13} dyne cm^{-2}. The assumed background gas pressure is based on the mean value observed in the outskirts of clusters and groups. See the *ACCEPT* database[12] for a catalog of such pressure profiles. Cavity ages were calculated assuming excavation at the gas sound speed. As a result of the radio lobes extending into regions where the pressure profiles are very steep and approaching the background pressure, the large volumes are offset by much lower pressures and longer ages, resulting in modest values of $P_{\rm cav}$.

Two of the PC sources, NGC 315 and NGC 4261, are part of a sample of nine FR-I objects analyzed in detail by Croston et al. (2008a, hereafter C08) using *XMM-Newton* X-ray observations. Provided in C08 are the $4pV$ enthalpies for each FR-I source (calculated using the radio lobe volumes and the external thermal pressure at the lobe mid-point), and the mean temperature of the group environments into which the lobes are expanding. Assuming lobe inflation occurs at the ambient gas sound speed, we calculated $P_{\rm cav}$ values for each of the C08 FR-I sources. For N315 and N4261 we find no significant difference between the $P_{\rm cav}$ values calculated using the *Chandra* data and the *XMM-Newton* data from C08. Using the NVSS search method outlined in Section 3.2 we calculated $P_{1.4}$ for each C08 FR-I source. Our PC objects and the C08 FR-I objects are plotted in Figure 2.

In Figure 2 we highlight the location of the PC sources relative to our best-fit 1.4 GHz relation and the W99 relation. Figure 2 shows that the PC and C08 FR-I sources reside well below our best-fit relation. This discrepancy implies that these sources have the lowest jet power per unit radio power of all objects in the sample. One explanation is that these sources may have lower k values, possibly because there are intrinsic differences in radio sources (light and heavy jets), or because all jets are born light and become heavy on large scales due to entrainment. Another explanation is that that PC sources are more powerful than our measurements indicate due to energy being imparted to shocks. On average, shock energy is a small correction to $P_{\rm cav}$, factor of a few in clusters (McNamara & Nulsen 2007), but the frequency and

[12] http://www.pa.msu.edu/astro/MC2/accept

variety of AGN driven shocks is broad, ranging from strong (Mach $\gtrsim 2$) – Centaurus A, NGC 3801 (Kraft et al. 2003; Croston et al. 2009, 2007) – to weak (Mach $\lesssim 2$) – 3C31, Cygnus A, Hydra A, Hercules A, M87, MS 0735.6+7421, NGC 4552, NGC 4636, NGC 4782 (Laing & Bridle 2002; Wilson et al. 2006; Wise et al. 2007; Nulsen et al. 2005; Forman et al. 2007; McNamara et al. 2005; Machacek et al. 2006; Baldi et al. 2009; Machacek et al. 2007) – to undetected – 3C 186, 3C 388, NGC 6764 (Siemiginowska et al. 2008; Kraft et al. 2006; Croston et al. 2008b). However, this explanation would require that the fraction of jet power going into shocks is preferentially higher for systems with relatively high implied radiative efficiencies (*i.e.* $P_{jet}/P_{radio} < \eta$).

5. SUMMARY AND CONCLUSIONS

We have presented analysis of the jet power versus radio power scaling relation for a sample of 21 giant elliptical galaxies observed with the *Chandra* X-ray Observatory. Cavity powers were calculated for each set of cavities using similar methods to those outlined in R06. Radio powers were estimated using 1.4 GHz and 200-400 MHz fluxes taken from the NVSS/SUMSS surveys and the CATS database.

Incorporating the data from B08, we find a continuous power-law relation between P_{jet}-P_{radio} covering 6 decades in P_{radio} and 8 decades in P_{jet} (Figure 1). We find similar forms for the power laws describing the P_{jet}-P_{radio} trend with the mean form $P_{jet} \approx 5.93 \times 10^{43}(P_{radio}/10^{40})^{0.68}$ erg s^{-1}, and a scatter about the fit of ≈ 0.7 dex. Our relations agree reasonably well with previous observational studies and predictions from theoretical jet models.

Several groups have applied the Bîrzan scaling relations to study the effects of AGN feedback on structure formation, *e.g.* Best et al. (2007) and Magliocchetti & Brüggen (2007), with some groups now suggesting that distributed low-power radio galaxies may dominate heating of the intracluster medium, *e.g.* Hart et al. (2009). Up to now, the available observational results, which were primarily calibrated to high-power radio sources, did not clearly indicate if a P_{jet}-P_{radio} relation would be continuous, or of comparable scatter, for lower power radio sources. Assuming there is no redshift evolution of P_{jet}-P_{radio}, our relations suggest higher mass galaxies dominate over lower mass galaxies in the process of mechanical heating within clusters. The next step is to study the process of mechanical heating in a cosmological context, *e.g.* evaluating the contribution of mechanically dominated AGN on the bolometric AGN luminosity function over cosmic time (Cattaneo & Best 2009).

We discussed a subset of objects that we classified as being poorly confined (PC) by their environments (Figure 2). These objects have P_{jet}/P_{radio} ratios which are large relative to the rest of our sample. In addition, PC sources reside in the same region of the P_{jet}-P_{radio} plane as the FR-I sources taken from C08. Possible explanations for the nature of these sources lie in the long-standing effort to understand the connection between properties of radio galaxies and their environment. Radio emission from lobes depends on their composition, so that the large scatter in the P_{jet}-P_{radio} relationship may result from processes such as gas entrainment and shocks. It seems likely that some of the scatter arises as radio sources age, but it remains unclear what other factors are important.

With tighter, self-consistent observational constraints on the P_{jet}-P_{radio} relation across several decades in both parameters, and host system mass, the need to rely on theoretical models to relate jet power to observed radio properties has weakened. Using P_{jet}-P_{radio} as an aide, a better understanding of the supermassive black hole power plants which underlie AGN activity can be undertaken. Moreover, future AGN feedback models, when used in simulations, must replicate the observed relations studied in this work.

KWC and BRM acknowledge generous support from the Natural Science and Engineering Research Council of Canada and grants from the *Chandra* X-ray Observatory. KWC sincerely thanks Judith Croston, David Rafferty, and Chris Willott for helpful insight. The *Chandra* X-ray Observatory Center is operated by the Smithsonian Astrophysical Observatory for and on behalf of NASA under contract NAS8-03060. The National Radio Astronomy Observatory is a facility of the National Science Foundation operated under cooperative agreement by Associated Universities, Inc. This research has made use of software provided by the *Chandra* X-ray Center, the NASA/IPAC Extragalactic Database operated by the California Institute of Technology Jet Propulsion Laboratory, and NASA's Astrophysics Data System. Some software was obtained from the High Energy Astrophysics Science Archive Research Center, provided by NASA's Goddard Space Flight Center.

Facilities: CXO (ACIS) VLA

REFERENCES

Akritas, M. G., & Bershady, M. A. 1996, ApJ, 470, 706 3
Baldi, A., Forman, W., Jones, C., Kraft, R., Nulsen, P., Churazov, E., David, L., & Giacintucci, S. 2009, ArXiv e-prints: 0909.2942 5
Begelman, M. C., & Cioffi, D. F. 1989, ApJ, 345, L21 3
Best, P. N., Kauffmann, G., Heckman, T. M., Brinchmann, J., Charlot, S., Ivezić, Ž., & White, S. D. M. 2005, MNRAS, 362, 25 1
Best, P. N., von der Linden, A., Kauffmann, G., Heckman, T. M., & Kaiser, C. R. 2007, MNRAS, 379, 894 5
Beuing, J., Dobereiner, S., Bohringer, H., & Bender, R. 1999, MNRAS, 302, 209 2
Birkinshaw, M., & Davies, R. L. 1985, ApJ, 291, 32 4
Birzan, L., McNamara, B. R., Nulsen, P. E. J., Carilli, C. L., , & Wise, M. W. 2010, The Astrophysical Journal, 709, 546 3
Bîrzan, L., McNamara, B. R., Nulsen, P. E. J., Carilli, C. L., & Wise, M. W. 2008, ApJ, 686, 859 1, 2, 4
Bîrzan, L., Rafferty, D. A., McNamara, B. R., Nulsen, P. E. J., & Wise, M. W. 2009, ArXiv e-prints: 0909.0397 1
Bîrzan, L., Rafferty, D. A., McNamara, B. R., Wise, M. W., & Nulsen, P. E. J. 2004, ApJ, 607, 800 1, 2
Blandford, R. D., & Konigl, A. 1979, ApJ, 232, 34 1, 4
Blandford, R. D., & Rees, M. J. 1974, MNRAS, 169, 395 3
Bock, D. C.-J., Large, M. I., & Sadler, E. M. 1999, AJ, 117, 1578 2
Bower, R. G., Benson, A. J., Malbon, R., Helly, J. C., Frenk, C. S., Baugh, C. M., Cole, S., & Lacey, C. G. 2006, MNRAS, 370, 645 1
Bridle, A. H., Davis, M. M., Fomalont, E. B., Willis, A. G., & Strom, R. G. 1979, ApJ, 228, L9 4
Carvalho, J. C., & O'Dea, C. P. 2002a, ApJS, 141, 337 3
—. 2002b, ApJS, 141, 371 3
Cattaneo, A., & Best, P. N. 2009, MNRAS, 395, 518 5
Cavagnolo, K. W., Donahue, M., Voit, G. M., & Sun, M. 2008, ApJ, 683, L107 1
—. 2009, ApJS, 182, 12 1
Cavaliere, A., & Fusco-Femiano, R. 1978, A&A, 70, 677 4
Condon, J. J. 1992, ARA&A, 30, 575 2
Condon, J. J., Cotton, W. D., Greisen, E. W., Yin, Q. F., Perley, R. A., Taylor, G. B., & Broderick, J. J. 1998, AJ, 115, 1693 2
Croston, J. H., Hardcastle, M. J., Birkinshaw, M., Worrall, D. M., & Laing, R. A. 2008a, MNRAS, 386, 1709 4, 8
Croston, J. H., Hardcastle, M. J., Kharb, P., Kraft, R. P., & Hota, A. 2008b, ApJ, 688, 190 5

Croston, J. H., Kraft, R. P., & Hardcastle, M. J. 2007, ApJ, 660, 191 5
Croston, J. H., Kraft, R. P., Hardcastle, M. J., Birkinshaw, M., Worrall, D. M., Nulsen, P. E. J., Penna, R. F., Sivakoff, G. R., Jordán, A., Brassington, N. J., Evans, D. A., Forman, W. R., Gilfanov, M., Goodger, J. L., Harris, W. E., Jones, C., Juett, A. M., Murray, S. S., Raychaudhury, S., Sarazin, C. L., Voss, R., & Woodley, K. A. 2009, MNRAS, 395, 1999 5
Croton, D. J., Springel, V., White, S. D. M., De Lucia, G., Frenk, C. S., Gao, L., Jenkins, A., Kauffmann, G., Navarro, J. F., & Yoshida, N. 2006, MNRAS, 365, 11 1
De Young, D. S. 2006, ApJ, 648, 200 4
De Young, D. S., O'Neill, S. M., & Jones, T. W. 2008, in Astronomical Society of the Pacific Conference Series, Vol. 386, Extragalactic Jets: Theory and Observation from Radio to Gamma Ray, ed. T. A. Rector & D. S. De Young, 343–+ 1
Diehl, S., & Statler, T. S. 2008, ApJ, 680, 897 1
Dunn, R. J. H., & Fabian, A. C. 2008, MNRAS, 385, 757 1
Dunn, R. J. H., Fabian, A. C., & Celotti, A. 2006, MNRAS, 372, 1741 4
Dunn, R. J. H., Fabian, A. C., & Taylor, G. B. 2005, MNRAS, 364, 1343 1, 4
Fabian, A. C., Sanders, J. S., Ettori, S., Taylor, G. B., Allen, S. W., Crawford, C. S., Iwasawa, K., Johnstone, R. M., & Ogle, P. M. 2000, MNRAS, 318, L65 1
Falcke, H., & Biermann, P. L. 1995, A&A, 293, 665 4
Falle, S. A. E. G. 1991, MNRAS, 250, 581 4
Ferrarese, L., & Merritt, D. 2000, ApJ, 539, L9 1
Forman, W., Jones, C., Churazov, E., Markevitch, M., Nulsen, P., Vikhlinin, A., Begelman, M., Böhringer, H., Eilek, J., Heinz, S., Kraft, R., Owen, F., & Pahre, M. 2007, ApJ, 665, 1057 5
Gallo, E., Fender, R. P., & Pooley, G. G. 2003, MNRAS, 344, 60 4
Gebhardt, K., Bender, R., Bower, G., Dressler, A., Faber, S. M., Filippenko, A. V., Green, R., Grillmair, C., Ho, L. C., Kormendy, J., Lauer, T. R., Magorrian, J., Pinkney, J., Richstone, D., & Tremaine, S. 2000, ApJ, 539, L13 1
Hart, Q. N., Stocke, J. T., & Hallman, E. J. 2009, ArXiv e-prints: 0908.3158 5
Heinz, S., & Grimm, H. J. 2005, ApJ, 633, 384 4
Heinz, S., & Sunyaev, R. A. 2003, MNRAS, 343, L59 4
Jones, D. L., & Wehrle, A. E. 1997, ApJ, 484, 186 4
Jones, D. L., Wehrle, A. E., Meier, D. L., & Piner, B. G. 2000, ApJ, 534, 165 4
Kauffmann, G., & Haehnelt, M. 2000, MNRAS, 311, 576 1
Killeen, N. E. B., & Bicknell, G. V. 1988, ApJ, 324, 198 4
Kormendy, J., & Richstone, D. 1995, ARA&A, 33, 581 1
Kraft, R. P., Azcona, J., Forman, W. R., Hardcastle, M. J., Jones, C., & Murray, S. S. 2006, ApJ, 639, 753 5
Kraft, R. P., Vázquez, S. E., Forman, W. R., Jones, C., Murray, S. S., Hardcastle, M. J., Worrall, D. M., & Churazov, E. 2003, ApJ, 592, 129 5
Laing, R. A., & Bridle, A. H. 2002, MNRAS, 336, 1161 5
Ledlow, M. J., & Owen, F. N. 1996, AJ, 112, 9 1
Longair, M. S., Ryle, M., & Scheuer, P. A. G. 1973, MNRAS, 164, 243 3
Machacek, M., Nulsen, P. E. J., Jones, C., & Forman, W. R. 2006, ApJ, 648, 947 5
Machacek, M. E., Kraft, R. P., Jones, C., Forman, W. R., & Hardcastle, M. J. 2007, ApJ, 664, 804 4, 5
Maglioccheti, M., & Brüggen, M. 2007, MNRAS, 379, 260 5
Magorrian, J., Tremaine, S., Richstone, D., Bender, R., Bower, G., Dressler, A., Faber, S. M., Gebhardt, K., Green, R., Grillmair, C., Kormendy, J., & Lauer, T. 1998, AJ, 115, 2285 1
Marconi, A., & Hunt, L. K. 2003, ApJ, 589, L21 1
Mathur, S., Stoll, R., Krongold, Y., Nicastro, F., Brickhouse, N., & Elvis, M. 2009, ArXiv e-prints: 0910.3691 1
Mauch, T., Murphy, T., Buttery, H. J., Curran, J., Hunstead, R. W., Piestrzynski, B., Robertson, J. G., & Sadler, E. M. 2003, MNRAS, 342, 1117 2
McNamara, B. R., & Nulsen, P. E. J. 2007, ARA&A, 45, 117 1, 4
McNamara, B. R., Nulsen, P. E. J., Wise, M. W., Rafferty, D. A., Carilli, C., Sarazin, C. L., & Blanton, E. L. 2005, Nature, 433, 45 3, 5
McNamara, B. R., Wise, M., Nulsen, P. E. J., David, L. P., Sarazin, C. L., Bautz, M., Markevitch, M., Vikhlinin, A., Forman, W. R., Jones, C., & Harris, D. E. 2000, ApJ, 534, L135 1
Merloni, A., & Heinz, S. 2007, MNRAS, 381, 589 4
Merloni, A., Heinz, S., & di Matteo, T. 2003, MNRAS, 345, 1057 4
Miley, G. 1980, ARA&A, 18, 165 4
Mittal, R., Hudson, D. S., Reiprich, T. H., & Clarke, T. 2009, A&A, 501, 835 1
Nulsen, P. E. J., Hambrick, D. C., McNamara, B. R., Rafferty, D., Bîrzan, L., Wise, M. W., & David, L. P. 2005, ApJ, 625, L9 3, 5
O'Sullivan, E., Ponman, T. J., & Collins, R. S. 2003, MNRAS, 340, 1375 2
Pellegrini, S., Venturi, T., Comastri, A., Fabbiano, G., Fiore, F., Vignali, C., Morganti, R., & Trinchieri, G. 2003, ApJ, 585, 677 4
Peterson, J. R., & Fabian, A. C. 2006, Phys. Rep., 427, 1 1
Pratt, G. W., Croston, J. H., Arnaud, M., & Böhringer, H. 2009, A&A, 498, 361 3
Puchwein, E., Sijacki, D., & Springel, V. 2008, ApJ, 687, L53 3
Rafferty, D. A., McNamara, B. R., & Nulsen, P. E. J. 2008, ApJ, 687, 899 1
Rafferty, D. A., McNamara, B. R., Nulsen, P. E. J., & Wise, M. W. 2006, ApJ, 652, 216 1, 2
Rawlings, S., & Saunders, R. 1991, Nature, 349, 138 1
Sanderson, A. J. R., O'Sullivan, E., & Ponman, T. J. 2009, MNRAS, 395, 764 1
Saro, A., Borgani, S., Tornatore, L., Dolag, K., Murante, G., Biviano, A., Calura, F., & Charlot, S. 2006, MNRAS, 373, 397 1
Scheuer, P. A. G. 1974, MNRAS, 166, 513 3
Schindler, S., Castillo-Morales, A., De Filippis, E., Schwope, A., & Wambsganss, J. 2001, A&A, 376, L27 1
Siemiginowska, A., LaMassa, S., Aldcroft, T. L., Bechtold, J., & Elvis, M. 2008, ApJ, 684, 811 5
Sijacki, D., & Springel, V. 2006, MNRAS, 366, 397 2
Sijacki, D., Springel, V., di Matteo, T., & Hernquist, L. 2007, MNRAS, 380, 877 1
Silk, J., & Rees, M. J. 1998, A&A, 331, L1 1
Verkhodanov, O. V., Trushkin, S. A., Andernach, H., & Chernenkov, V. N. 1997, in Astronomical Society of the Pacific Conference Series, Vol. 125, Astronomical Data Analysis Software and Systems VI, ed. G. Hunt & H. Payne, 322–+ 3
Weinmann, S. M., van den Bosch, F. C., Yang, X., Mo, H. J., Croton, D. J., & Moore, B. 2006, MNRAS, 372, 1161 3
Weisskopf, M. C., Tananbaum, H. D., Van Speybroeck, L. P., & O'Dell, S. L. 2000, in Presented at the Society of Photo-Optical Instrumentation Engineers (SPIE) Conference, Vol. 4012, Proc. SPIE Vol. 4012, p. 2-16, X-Ray Optics, Instruments, and Missions III, Joachim E. Truemper; Bernd Aschenbach; Eds., ed. J. E. Truemper & B. Aschenbach, 2–16 1
Whiteoak, J. B. 1970, Astrophys. Lett., 5, 29 2
Willis, A. G., Strom, R. G., Bridle, A. H., & Fomalont, E. B. 1981, A&A, 95, 250 4
Willott, C. J., Rawlings, S., Blundell, K. M., & Lacy, M. 1999, MNRAS, 309, 1017 1, 4, 8
Wilson, A. S., Smith, D. A., & Young, A. J. 2006, ApJ, 644, L9 3, 5
Wise, M. W., McNamara, B. R., Nulsen, P. E. J., Houck, J. C., & David, L. P. 2007, ApJ, 659, 1153 3, 5

TABLE 1
SUMMARY OF SAMPLE

Source	R.A.	Decl.	D_C	$P_{1.4}$	$P_{200-400}$	$P_{\rm cav}^{\rm buoy}$	$L_{\rm X}(< r_{\rm cool})$	FM
-	hr:min:sec	° : ′ : ″	Mpc	10^{38} erg s^{-1}	10^{38} erg s^{-1}	10^{42} erg s^{-1}	10^{33} erg s^{-1}	–
(1)	(2)	(3)	(4)	(5)	(6)	(7)	(8)	(9)
IC 4296†	13:36:39	-33:57:57	53	38.5 ± 3.4	218 ± 18	$3.87^{+1.44}_{-3.03}$	18.6	B
NGC 315†	00:57:48	+30:21:09	70	56.7 ± 5.1	20.6 ± 0.2	$6.58^{+2.48}_{-4.96}$	28.8	B
NGC 507	01:23:39	+33:15:22	70	0.845 ± 0.039	1.33 ± 0.13	$19.9^{+4.4}_{-6.8}$	1090	B
NGC 777	02:00:14	+31:25:45	71	0.0614 ± 0.0044	0.0482 ± 0.0048	$4.08^{+1.48}_{-3.03}$	98.5	C
NGC 1316	03:22:41	-37:12:28	25	0.273 ± 0.011	0.0601 ± 0.0091	$1.11^{+0.26}_{-0.40}$	5.93	B
NGC 1553	04:16:10	-55:46:48	15	0.0027 ± 0.0004	0.1395 ± 0.0465	$0.98^{+0.34}_{-0.70}$	172	C
NGC 1600	04:31:39	-05:05:10	67	0.471 ± 0.019	···	$1.87^{+0.82}_{-2.00}$	11.6	B
NGC 3608	11:16:58	+18:08:54	18	0.0014 ± 0.0001	0.0206 ± 0.0001	$0.05^{+0.02}_{-0.03}$	0.783	C
NGC 4261†	12:19:23	+05:49:29	32	18.2 ± 0.6	62.9 ± 6.7	$0.91^{+0.37}_{-0.79}$	7.57	B
NGC 4374	12:25:03	+12:53:13	15	2.31 ± 0.08	1.21 ± 0.05	$5.03^{+2.17}_{-5.53}$	7.58	A
NGC 4472	12:29:46	+08:00:02	14	0.0860 ± 0.0034	0.0684 ± 0.0098	$0.53^{+0.16}_{-0.32}$	16.1	A
NGC 4552	12:35:39	+12:33:23	4.7	0.0037 ± 0.0001	···	$0.53^{+0.12}_{-0.17}$	2.22	A
NGC 4636	12:42:49	+02:41:16	13	0.0231 ± 0.0008	0.0690 ± 0.0005	$2.76^{+0.56}_{-0.91}$	37.6	B
NGC 4782†	12:54:35	-12:34:07	66	57.4 ± 1.8	66.6 ± 6.7	$2.43^{+0.86}_{-1.43}$	13.9	B
NGC 5044	13:15:23	-16:23:07	39	0.0874 ± 0.0028	0.0192 ± 0.0019	$4.18^{+1.18}_{-1.97}$	425	B
NGC 5813	15:01:11	+01:42:07	28	0.0200 ± 0.0014	0.256 ± 0.041	$3.97^{+1.02}_{-2.36}$	180	A
NGC 5846	15:06:29	+01:36:20	24	0.0211 ± 0.0013	0.0584 ± 0.0001	$0.88^{+0.30}_{-0.59}$	64.4	B
NGC 6269	16:57:58	+27:51:15	150	1.95 ± 0.074	···	$1.54^{+0.49}_{-1.03}$	118	C
NGC 6338	17:15:22	+57:24:40	120	1.37 ± 0.043	0.441 ± 0.044	$11.0^{+3.3}_{-6.9}$	388	B
NGC 7626†	23:20:14	+08:12:23	49	3.42 ± 0.13	···	$0.39^{+0.09}_{-0.18}$	11.5	B
UGC 408	00:39:18	+03:19:52	63	8.65 ± 0.28	6.13 ± 0.32	$9.99^{+3.12}_{-4.54}$	45.7	A

NOTE. — A dagger (†) indicates a poorly confined radio source (see Section 4.3) which is not plotted in Figure 1. Col. (1) Source name; Col. (2) R.A. of source centroid; Col. (3) Decl. of source centroid; Col. (4) Comoving distance; Col. (5) 1.4 GHz radio power; Col. (6) 200-400 MHz radio power; Col. (7) Cavity power calculated using buoyancy age; Col. (8) X-ray luminosity (0.3-2.0 keV) within radius where $t_{\rm cool} \leq 7.7$ Gyrs; Col. (9) Figure of merit (FM) assigned to quality of cavity system (see Section 4).

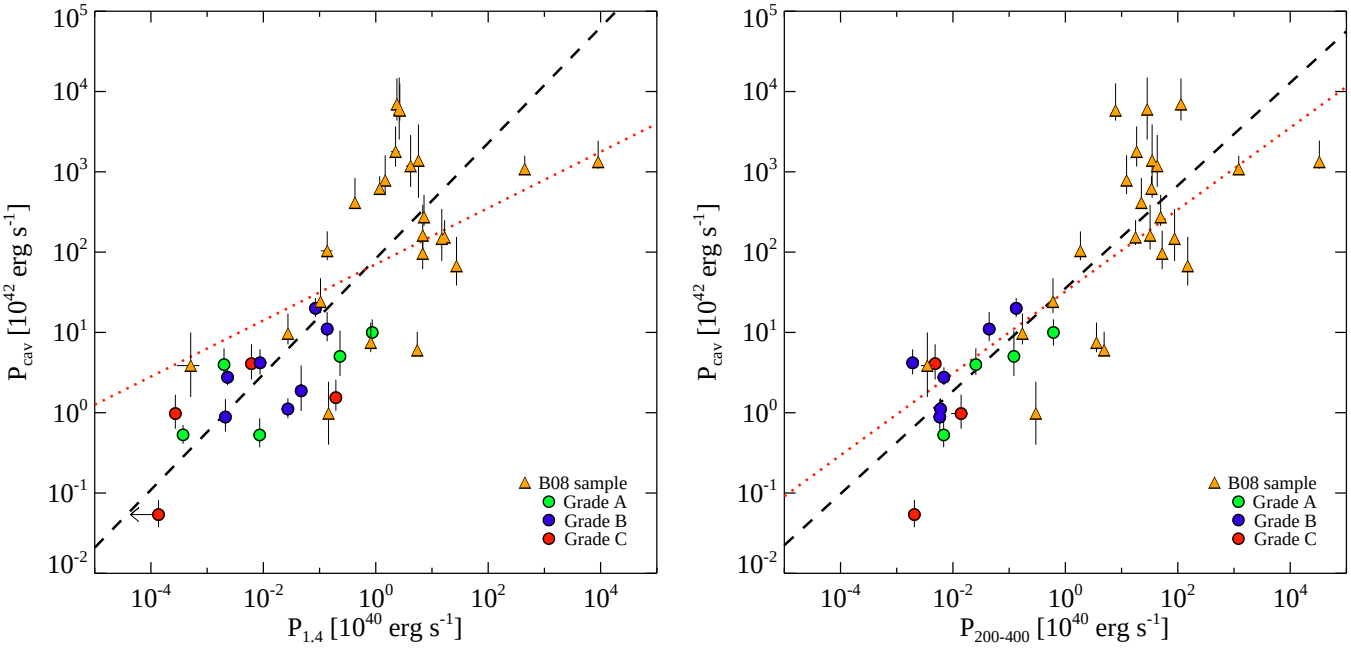

FIG. 1.— Cavity power vs. radio power. Orange triangles represent the galaxy clusters and groups sample from B08. Filled circles represent our sample of gEs with colors representing the cavity system figure of merit (see Section §3.1): green = 'A,' blue = 'B,' and red = 'C.' The dotted red lines represent the best-fit power-law relations presented in B08 using only the orange triangles. The dashed black lines represent our BCES best-fit power-law relations. *Left:* Cavity power vs. 1.4 GHz radio power. *Right:* Cavity power vs. 200-400 MHz radio power.

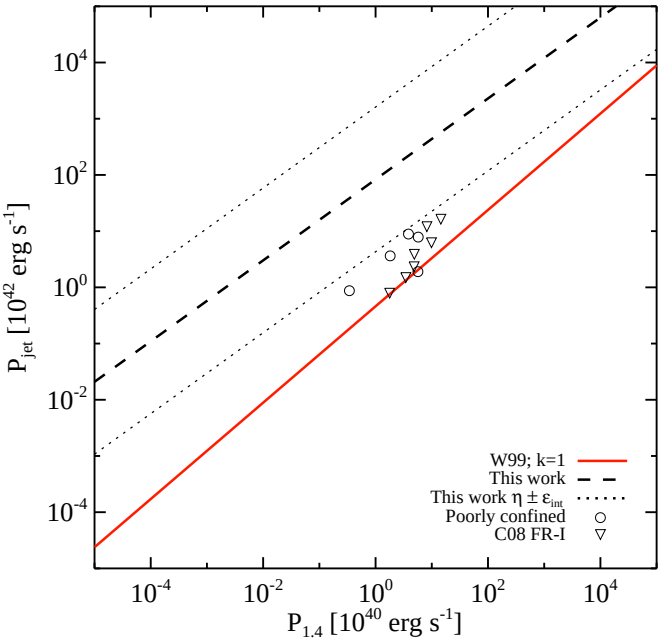

FIG. 2.— Comparison of scaling relations between jet power and radio luminosity. The solid red line represents the Willott et al. (1999, W99) model with $k = 1$. The dashed black line is our best-fit P_{jet}-$P_{1.4}$ relation (Equation 1). The dotted black lines denote the upper and lower limits of our best-fit relation after including intrinsic scatter of $\epsilon_{int} = 1.3$ dex. The unfilled black circles denote the poorly confined sources discussed in Section 4.3, and the downfacing black triangles are FR-I sources taken from the sample in Croston et al. (2008a, C08).

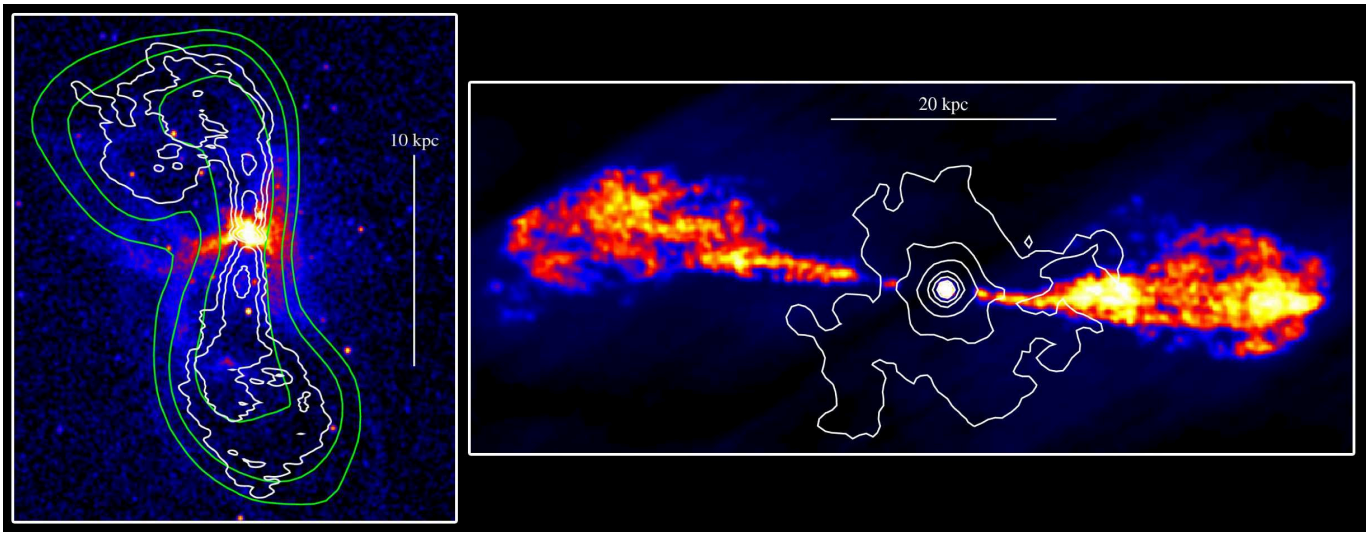

FIG. 3.— *Left: Chandra* X-ray image of the giant elliptical M84 (NGC 4374). Contours trace out 1.4 GHz radio emission as observed with VLA C-configuration (green) and AB-configuration (white) ranging from $\approx 0.5-50$ mJy in log spaced steps of 10 mJy. Note the displacement of the X-ray gas around the bipolar AGN jet outflows. M84 is an excellent example of a typical interaction between an AGN outflow and a hot gaseous halo. *Right:* VLA B-configuration 1.4 GHz radio image of the AGN jets eminating from the giant elliptical NGC 4261. White contours trace *Chandra* observed X-ray emission of the hot halo surrounding N4261. The contours cover the surface brightness range of $\approx 5-50$ cts arcsec^{-2} in linear spaced steps of 5 cts arcsec^{-2}. N4261 demonstrates the characteristic traits of what we have termed poorly confined sources: a compact X-ray halo, small centralized cavities along the jets, FR-I-like radio morphology, and pluming beyond the "edge" of the X-ray halo.